Desalination and Water Treatment
www.deswater.com
doi: 10.5004/dwt.2019.24128

157 (2019) 1–7
July

Study on liquid film thickness and flow characteristics of falling film outside an elliptical tube

Xiaocui Zhang, Xiaojing Zhu, Qinggang Qiu*

School of Energy and Power, Dalian University of Technology, Dalian, 116024, China, Tel. +13591105818; email: qqgang@dlut.edu.cn (Q. Qiu), Tel. +13555936530; email: 1457997450@qq.com (X. Zhang), Tel. +18642809658; email: zhuxiaojing@dlut.edu.cn (X. Zhu)

Received 10 October 2018; Accepted 16 March 2019

ABSTRACT

A three-dimensional model is applied to simulate the spreading process and thickness distribution of the liquid film outside an elliptical horizontal tube falling-film heat exchanger. Reynolds number (Re) is 187 and the counter-current air flow rates are 0, 0.1 and 0.5 m/s, respectively. The volume of fluid method is used to trace the gas–liquid interface. It is shown that falling film flow delays and the liquid film thickness increases as the gas flow rate increases. When the counter-current gas flow rate is increased to 0.5 m/s, the falling film distribution becomes uneven and local accumulation occurs. Along the circumferential direction, the liquid film velocity increases as the gas flow rate increases.

Keywords: Numerical simulation; Liquid film thickness; Liquid film velocity; Counter-current air

1. Introduction

Horizontal tube falling film evaporation has a wide range of applications, including seawater desalination, petrochemical industry, and air conditioning and refrigeration. It is an efficient heat-exchange technology in which high temperature steam releases heat by evaporation outside the horizontal tubes. Until now, there are so many researches carried out to study the flow patterns in the horizontal tube falling film evaporator.

Mu et al. [1,2] and Shen et al. [3,4] conducted a comprehensive study on the flow characteristics and heat transfer efficiency of fluids in falling film evaporators. They also studied in detail the various factors affecting heat transfer, such as heat flux density, number of tubes, spray density, evaporation temperature, etc., and studied the difference in heat transfer between seawater and freshwater as experimental fluids. Hou et al. [5] used a displacement micrometer to measure the thickness of the liquid film in the range of 15°–165° around the circumferential angle of the tube. Experimental analysis found that the film thickness is mainly affected by the circumferential angle of the tube wall, the tube spacing and the Re number. The minimum thickness of the circumferential liquid film thickness does not always appear at 90°, but in the range of 90°–115°. Han and Shikazono [6] used a laser focus displacement meter to measure the liquid film thickness of the droplet on the surface of the micro-tube. The diameter of the tube was from 0.3 to 1.3 mm. The droplets were made of water, ethanol and fluoridate. The micro-measurement results show that the change of the liquid film thickness value with the circumferential angular position is mainly caused by the force component of gravity; the effect of Reynolds number on the liquid film thickness is very large, and when Re is greater than 2,000, the droplet will continuously fall or even occur sputtering. Fiorentino and Starace [7] and Jahangeer et al. [8] numerically studied the falling film flow characteristics under consideration of the upward blowing of the bottom of the horizontal tube. In addition, they also carried out a more comprehensive simulation of liquid spray density, air flow rate and tube row mode. Xu et al. [9] experimentally studied the factors affecting the flow pattern outside the tube. They

* Corresponding author.

found that the number of spray Re corresponding to the drop pattern is about 400; the column pattern corresponded spray Re number range is 400–1,600; as the spray Re number is higher than 1,600, the sheet pattern appears between the tubes. Elshazly et al. [10] studied the effect of angle of attack on the natural convective heat transfer rate in an elliptical tube. Under the same Rayleigh number, the average Nusselt number increases with the increase of the angle of attack. Esfahani and Modirkhazeni [11] used numerical methods to study the effects of ellipticity, Re number and Brinkman number on the entropy production of the liquid heat transfer process outside the horizontal elliptical tube. Qi et al. [12] studied the heat transfer of the outer liquid film outside elliptical tube. The experimental results show that heat transfer coefficient of the elliptical tubes with ellipticity = 1.5 higher than circular tubes. Qiu et al. [13] simulated the effect of tube shape on the thickness and heat transfer of falling film outside the horizontal tubes, the results show that the film thickness outside the elliptical tube is more unique compared with that of a circular tube, and the heat transfer of falling film outside elliptical tube is better. Tan and Jiang [14] also simulated the characteristic of falling film outside the elliptical tube, they found that the liquid rate in the elliptical tube is faster than in the round tube, and the heat transfer performance of the elliptical is optimal with the ellipticity = 1.65. Peng et al. [15] according to the digital image process obtained that in the same condition, the average of semi-elliptical tube is minimum, compared with the round tune and the elliptical tube of the same section circumference. Asbik et al. [16] observed in their study that the decreasing ellipticity generates a noticeable reduction in the laminar sublayer and hence favors the turbulence regime. Lee et al. [17] simulated the effect of obliquely dispensed angle on heat transfer of elliptical tube. They found that increasing the obliquely dispensed angle can result in angle thinner liquid films, lower interfacial velocities and worse heat transfer outcomes, also they think the reasonable obliquely dispensed angle is within 30°.

The above researches mainly studied the effect of Re number and geometric parameters on the falling film flow characteristics and heat transfer of falling film under the static environment, and rarely studies the influence of the air flow on the flow characteristics of the falling film outside the elliptical tube. In this paper, the effects of a counter-current flow on the flow characteristics of the falling film outside the elliptical tube and the thickness of the liquid film are studied by three-dimensional numerical simulation.

2. Computational method

2.1. Physical model and grid model

During the falling of the horizontal pipe, the liquid flows along the pipe wall and exhibits different flow models under different spray density phases. The ideal flow pattern of the horizontal tube falling film flow is divided into three types: droplet flow, column flow and curtain flow. The flow state simulated in this paper is a columnar flow with a flow of Re = 187.

The physical model of this paper is as follows: the spray liquid is sprayed from the nozzle to the horizontal tube under the action of gravity, and then a liquid film is formed outside the horizontal tube, and the liquid film spreads on the surface of the tube in the axial direction and the circumferential direction until the tube wall is completely wet. The liquid will accumulate at the bottom of the tube and form a new liquid column at the point where it will flow, and the liquid column will flow to the next tube. The process of liquid film diffusion is affected by gravity, surface tension, viscous force and gas–liquid shear force. The axial range of the calculation domain is the distance between the two spray ports, the spray port is in the middle position, the diameter D = 2 mm, and the spray speed V_i = 0.6 m/s. Both sides have symmetrical boundary conditions. The elliptical tube has a long semi-axis A = 26 mm, a short half-axis B = 13 mm, a longitudinal tube spacing $H1$ = 50 mm, and a lateral tube spacing $H2$ = 34 mm.

In this paper, a mesh model is built by The Integrated Computer Engineering and Manufacturing code (ICEM). In order to obtain a high-quality mesh, the O mesh and the boundary layer mesh are used to divide the mesh. Encryption is performed close to the wall area to accurately capture the gas–liquid interface. The mesh model and boundary conditions are shown in Fig. 1. In order to save computation time and meet the calculation accuracy, the number of grids is 500 W and the calculation time step is 0.5 ms.

2.2. Assumed condition and the liquid propriety

The main research purpose of this paper is to obtain the flow behavior and film formation law of falling film liquid outside the tube. The simulation work is based on the following basic assumptions:

- The falling film flow is laminar flow, and the fluid is continuously incompressible. The liquid phase in this simulation is liquid water at normal temperature and normal pressure, and the gas phase is an ideal gas at normal temperature and pressure, and the physical parameters are constant.
- The tube wall is initialized to a completely wet state, so the wall contact angle is set to 0°.
- Heat transfer is not considered.
- The pipe wall is a non-slip wall boundary.

In this paper, the physical parameters of gas–liquid two phases are provided in Table 1.

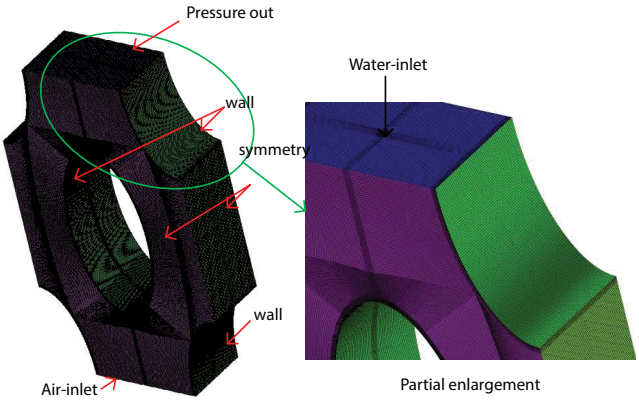

Fig. 1. Physical model.

Table 1
Fluid properties

	Density (kg/m^3)	Viscosity (k/(m s))	Surface tension (N/m)
Water	998.2	1×10^{-3}	0.073
Air	1.225	1.7894×10^{-4}	–

2.3. Mathematical model

The Re number of liquid film flow studied in this paper is 187, and the laminar flow state is set when solving. Numerical simulation selected the volume of fluid (VOF) model to dynamically capture the interface between gas and liquid two phases to better obtain the gas–liquid two-phase interface. The VOF method is a method of defining a gas–liquid interface by calculating the volume fraction F (volume fraction) of each phase in each grid cell. The volume fraction of each phase in the grid unit ranges from 0 to 1, that is, when the volume fraction of a phase is 1, it means that the grid unit is completely filled with the fluid; when the volume fraction of a phase is 0, that indicates that there is no such fluid in the grid unit, and another fluid is filled with the grid unit.

In VOF, different phases (different fluids) share a set of governing equations. The mass conservation equations and momentum equations of each phase can be expressed as follows:

$$\nabla \vec{v} = 0 \tag{1}$$

$$\frac{\partial \rho \vec{v}}{\partial t} + \nabla \times \left(\rho \vec{v} \otimes \vec{v} - \vec{T}\right) = \rho \vec{g} + \vec{f}_{\sigma} \tag{2}$$

$$\vec{f}_{\sigma} = -\left(\sigma \nabla_{\alpha}\right) \nabla \times \left(\frac{\nabla_{\alpha}}{\left|\nabla_{\alpha}\right|}\right) \tag{3}$$

where σ is surface tension.

The content of this paper is gas–liquid two-phase flow, defining air as the first phase and liquid water as the second phase. The equation for solving VOF is as follows:

$$\frac{\partial \alpha_2}{\partial t} + \vec{v} \times \nabla \partial_2 = 0 \tag{4}$$

where the volume fraction of each phase fluid is the velocity vector.

Since each grid unit is necessarily composed of gas and liquid, the volume fraction of both is always 1. Therefore, after obtaining the volume fraction of one phase by the above formula, the volume fraction of the other phase is given by:

$$\alpha_1 = 1 - \alpha_2 \tag{5}$$

The fluid density in each grid can be obtained by weighted averaging:

$$\rho = \alpha_2 \rho_l + \left(1 - \alpha_2\right) \rho_g \tag{6}$$

The dynamic viscosity in the grid unit can be expressed as:

$$\mu = \alpha_2 \mu_1 + \left(1 - \alpha_2\right) \mu_g \tag{7}$$

3. Results and discussions

3.1. Influence on the process of the liquid film

Fig. 2 shows the transient process of the liquid film outside the horizontal elliptical tube in static environment at Re = 187. When the liquid flows out of the velocity inlet, it begins to fall under the force of gravity and surface tension, and the lower end of the liquid appears spherical (Fig. 2a1), and the liquid column is gradually stretched and thinned during the falling process. At about 0.07 s, the liquid began to touch the wall of the horizontal tube and began to spread along the axial direction (Fig. 2a2). The impact of the falling liquid on the wall of the tube will cause strong liquid film fluctuations in the previously formed liquid film. This strong disturbance will increase the heat transfer coefficient during heat transfer and is beneficial to heat transfer. Thereafter, the liquid film starts to spread simultaneously in the circumferential direction and the axial direction of the cross tube, and a plurality of superimposed external forces and liquid internal forces simultaneously act on the liquid outside the tube (Fig. 2a3). When t = 0.45 s, the liquid film touches the bottom of the tube (Fig. 2a4), and the liquid film formed on the tube wall fluctuates due to the change in the flow velocity. The liquid film flows to the bottom of the tube and gradually gathers together at both ends of the elliptical tube. As the pooling liquid increases, the vertical gravity of the liquid is also increased. The liquid at the bottom will detach from the wall and fall down. The liquid that has escaped from the flow will be elongated and thinned during the falling process, forming two new liquid columns to continue to flow to the next heat exchange tube or into the storage tank (Fig. 2a5).

Fig. 3 shows the transient process of the liquid film outside the horizontal elliptical tube at different velocity of counter-current air flow. Compared with Fig. 2, it can be seen that the counter-current flow caused a delay in the fluid landing, and it was obvious that a large sphere was formed at the bottom of the liquid column (Figs. 3b1, b2, c1–c3). That is the gas–liquid shear force under the counter-current gas flow condition is greater than that without the gas flow, and the gas–liquid shear force is opposite to the fluid flow direction, so the fluid flows downward against the shear force, thus causing a hysteresis effect. It can be seen from Figs. 3b4 and c4 that the new liquid column has a tendency to flow upward due to the influence of the counter-current gas flow. In Figs. 3b5 and c5, it can be seen that the fluid has flowed upward and the crushing effect is generated. This is because the velocity of the gas flow is relatively large near the gas inlet, so that the effect of the gas–liquid shear force is greater than the action of gravity, thus causing a counter-current effect of the fluid.

3.2. Influence on the thickness of the liquid film

The liquid film thickness as one of the main influencing factors of heat transfer strength is one of the criteria for measuring the heat transfer performance. In order to study

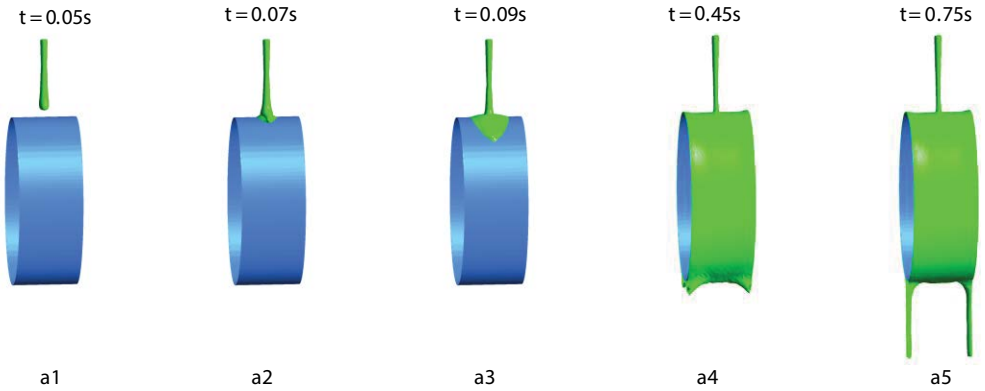

Fig. 2. Transient process of the liquid film outside the horizontal elliptical tube in static environment.

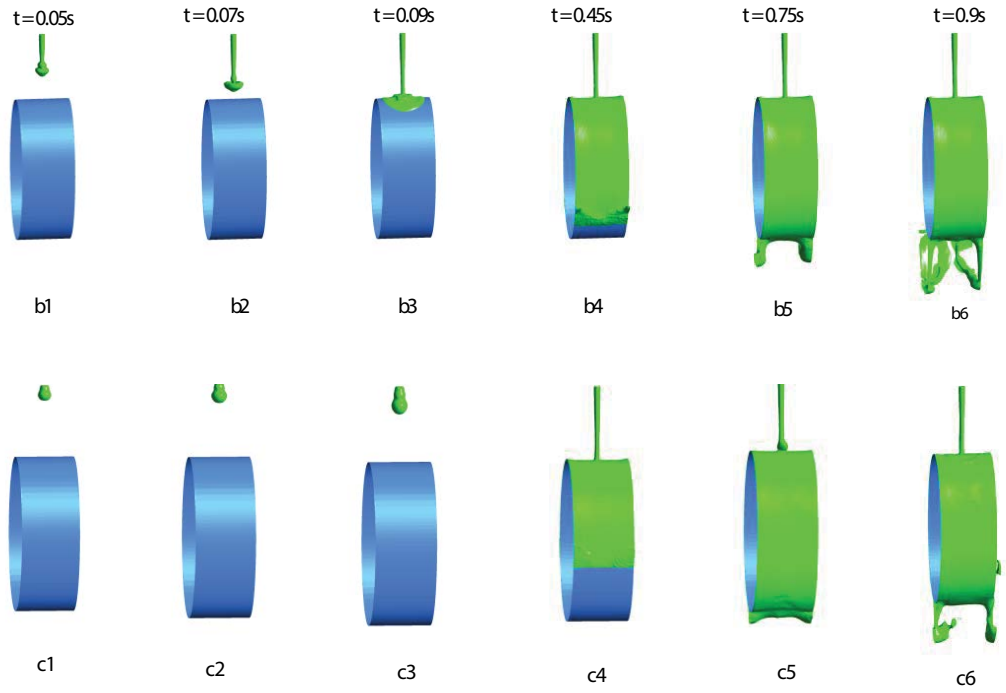

Fig. 3. Transient process of the liquid film outside the horizontal elliptical tube, ((b1)–(b6)) V_{air} = 0.1 m/s, ((c1)–(c6)) V_{air} = 0.5 m/s.

the distribution of the liquid film in the axial direction and the circumferential direction, a plane was selected at the axial distance of the top of the elliptical wall of the research unit, and the liquid film thickness distribution was analyzed. The dimensionless distance L^* is defined as follows:

$$L^* = \frac{L}{\lambda} \tag{8}$$

where λ is the sprinkler spacing, and the value under current conditions is 20 mm; L is the distance from the measuring point to the leftmost symmetry plane.

Fig. 4 shows the liquid film thickness distribution outside the horizontal elliptical tube at V_{air} = 0 m/s. The thickness of the liquid film at each position (L^* = 0, 1, 0.1, 0.9) generally shows a trend of decreasing first and then decreasing, and then increasing again. In the range of 5°–10° of the circumferential angle, the thickness of the liquid film increases due to the impact of the liquid column. In the range of 10°–45°, the liquid film begins to spread rapidly along the circumference and axial direction, and the thickness of the liquid film rapidly decreases. In the range of 45°–90°, the thickness of the liquid film is slowly reduced until the minimum thickness of the liquid film is reached, and then the thickness of the liquid is gradually increased due to the force of gravity in the tangential direction. In the range of 165°–170°, the liquid is stretched due to the convergence of the bottom portion of the liquid column and the interaction between the liquids. The liquid film thickness is lower in the range of 170°, and then the new liquid is concentrated at the bottom of the heat exchange tube. At the other position (L^* = 0.2–0.8), the liquid film gradually increases in the range of 5°–30° in the circumferential angle until the 30 reaches a larger value. That is the liquid column freely falls to the

elliptical tube top tube at the section L^* = 0.5, spreading along the axial and axial directions, and the axial L^* = 0.2–0.8 direction is more affected by the liquid column impact, so the liquid film of the tube gradually increases and is smaller than the thickness of the liquid film at both ends of the axial direction.

Also, it can be seen from Fig. 4, at the same circumferential angular position, the thickness of the liquid film also varies greatly along different axial positions. The film thickness of the circumferential angle on the axial slice of both sides of the slice L^* = 0.5 is symmetrically distributed. The thickness of the liquid film at the axial intermediate position L^* = 0.5 is the smallest, and the thickness of the liquid film at both ends in the axial direction gradually increases.

Fig. 5 shows the liquid film thickness distribution outside the horizontal elliptical tube at V_{air} = 0.1 m/s. It can be seen that the change trend in the circumferential direction and the axial direction is similar to the liquid film thickness change trend in the absence of air flow. However, the range of variation of the liquid film thickness in the axial direction is reduced due to an increase in gas–liquid shear force. It can be seen from the figure that in the range of 90°–170°, the liquid film thickness of Fig. 5 is higher than that of the liquid film thickness of Fig. 4, because the direction of gas–liquid shear force is opposite to the direction of fluid flow, which hinders the fluid flows downward, and causes the thickness of the liquid film to increase. And it can be seen from the figure that due to the action of the gas–liquid shear force, there is a slight upward movement at the minimum point of the liquid film thickness in the circumferential spreading area, which is not a significant 90°.

Fig. 6 shows the liquid film thickness distribution outside the horizontal elliptical tube at V_{air} = 0.5 m/s. It can be seen that at a circumferential angle of 135°, due to the sweeping of the counter-current air flow, liquid film accumulation occurs, and the thickness of the liquid film sharply increases and the maximum can reach 2.2 mm. At the other positions, the liquid film thickness is less than 0.8 mm. Compared with Figs. 4 and 5, the average liquid film thickness becomes larger, and no certain law. In the axial direction, the thickness of the liquid film is thick at both sides and is thin at the middle.

3.3. Influence on the velocity of the liquid film in water–air interface

Fig. 7 shows the contour of the velocity along the circumferential direction at different velocity of the counter-current air flow in the plane of L^* = 0.5. It can be seen that the airflow diffuses along the circumferential direction of the tube, which has a greater influence on the fluid at the bottom of the horizontal tube. With the increase of airflow velocity, the influence of airflow on the falling film flow field is gradually increased. When the airflow velocity is increased to 0.5 m/s, the flow velocity of large area can reach 0.96 m/s.

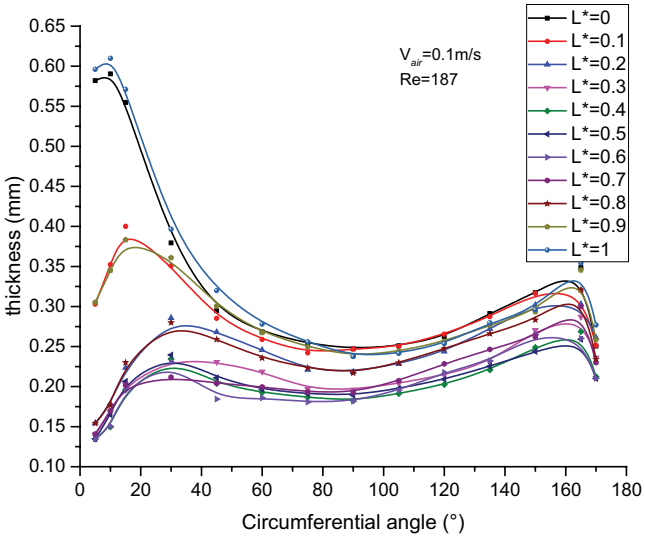

Fig. 5. Liquid film thickness distribution outside the horizontal elliptical tube at V_{air} = 0.1 m/s.

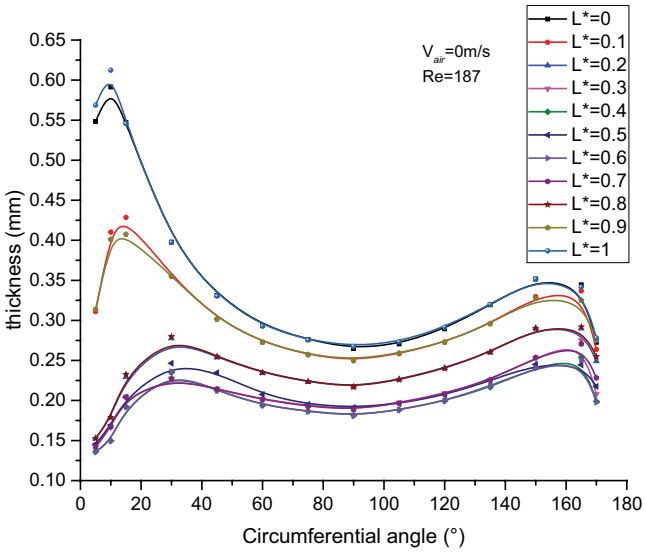

Fig. 4. Liquid film thickness distribution outside the horizontal elliptical tube at V_{air} = 0 m/s.

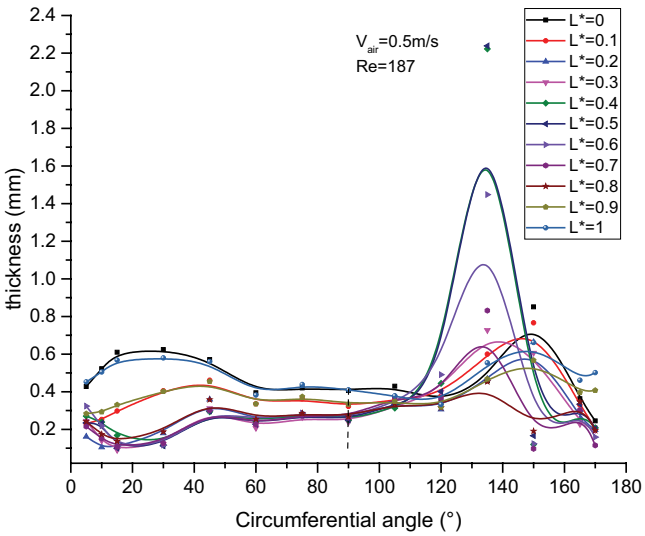

Fig. 6. Liquid film thickness distribution outside the horizontal elliptical tube at V_{air} = 0.5 m/s.

Fig. 8 shows the velocity in water–air interface along the circumferential direction at different velocity of the counter-current air flow in the plane of $L^* = 0.5$. It can be seen that along the circumferential direction, the liquid film flow velocity in water–air interface increases with the gas flow rate increasing. As $V_{air} = 0$ m/s, the falling film flow velocity decreases along the circumferential direction in the range of 0°–15°. When $V = 0$, in the range of 0°–15°, the falling film flow velocity decreases along the circumferential direction due to the effect of the liquid column impact, and remains substantially unchanged after 15°. As $V_{air} = 0.1$ m/s, the influence of the liquid column impact increases to 30°. As $V_{air} = 0.5$ m/s, the falling film flow velocity decreases first and then increases slowly, and the influence of the liquid column impact also reaches 30°.

Fig. 9 shows the contour of the velocity along the circumferential direction at different velocity of the counter-current air flow in the plane of $L^* = 1$. It can be seen that flow field dramatically changes as the airflow velocity increases, and the farther away from the elliptical tube, the greater the airflow effect. The fluid at the upper of the elliptical tube is less affected. But the fluid at the bottom of the elliptical tube is purged by a counter-current flow, and flow upward.

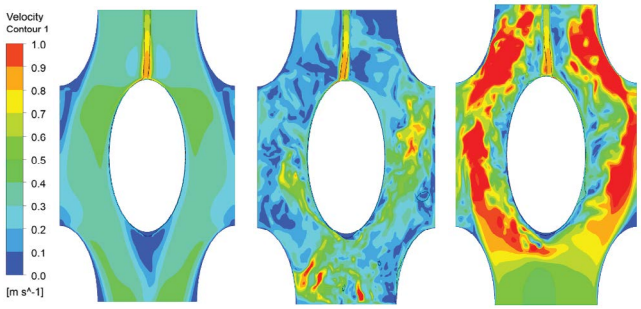

Fig. 7. Contour of the velocity along the circumferential direction in $L^* = 0.5$. (a) $V_{air} = 0$ m/s; (b) $V_{air} = 0.1$ m/s; and (c) $V_{air} = 0.5$ m/s.

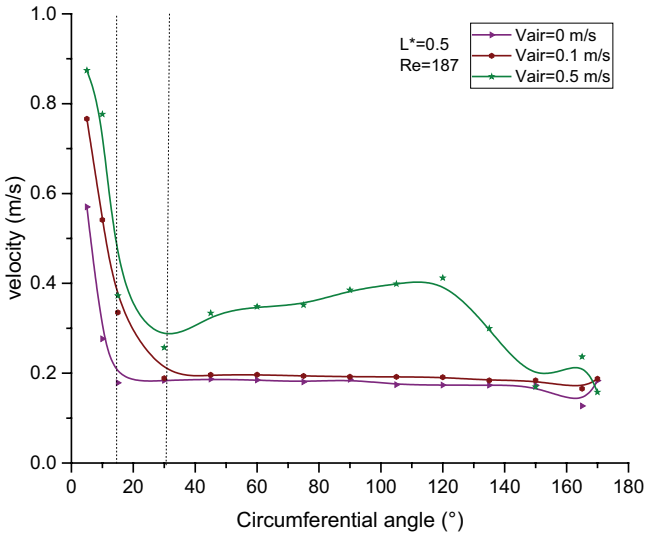

Fig. 8. Velocity in water–air interface outside the horizontal elliptical tube in $L^* = 0.5$.

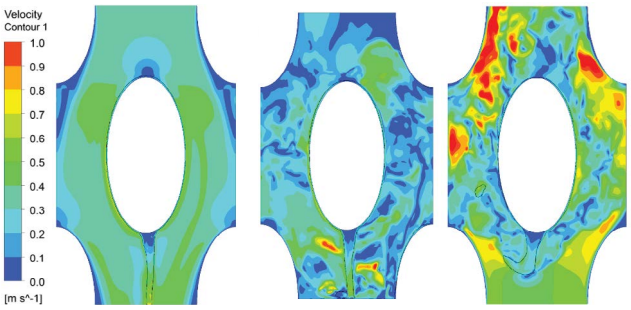

Fig. 9. Contour of the velocity along the circumferential direction in $L^* = 1$. (a) $V_{air} = 0$ m/s; (b) $V_{air} = 0.1$ m/s; and (c) $V_{air} = 0.5$ m/s.

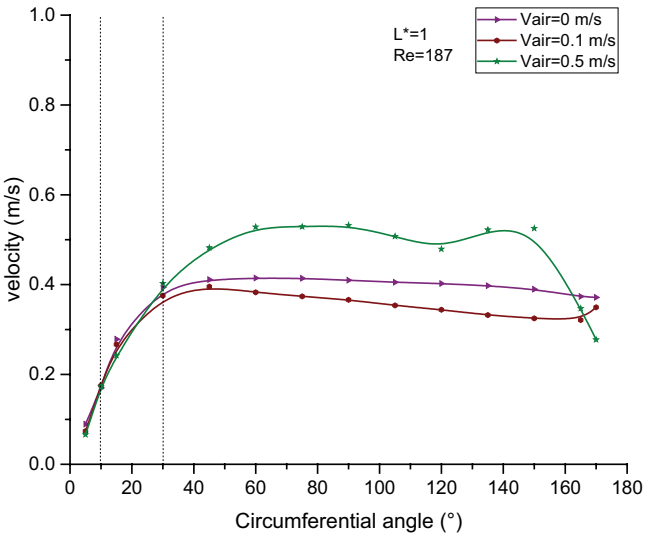

Fig. 10. Velocity in water–air interface outside the horizontal elliptical tube in $L^* = 1$.

Fig. 10 shows the velocity in water–air interface along the circumferential direction at different velocity of the counter-current air flow in the plane of $L^* = 1$. It can be seen that the liquid film flow rate gradually increases along the circumferential direction before 30°. After 30°, along the circumferential direction, the falling film velocity slowly decreases at $V_{air} = 0$ m/s, and basically unchanged at $V_{air} = 0.1$ m/s, and continue to increase at $V_{air} = 0.5$ m/s. Before 10°, the fluid falling film flow velocities at different counter-current air flow rates are the same along the circumferential direction. It is noted that the effect of counter-current flow is small before the circumferential angle is 30°.

4. Conclusion

In this paper, a three-dimensional numerical simulation is used to simulate the flow characteristics and liquid film thickness distribution of the outer elliptical tube with counter-current flow velocity. According to the simulation conditions in the paper, the following conclusions are obtained:

- The counter-current flow delays the falling film flow process, the greater the air flow velocity, the more the delay,

and the more unstable the falling film. Near the entrance of the air flow, the fluid accumulates at the bottom of the elliptical tube and even flow in the opposite direction.
- The thickness of the liquid film outside the elliptical tube is first increased and then decreased, and then increased. The minimum liquid film thickness is 90° in the circumferential angle. The thickness of the liquid film becomes larger with the air flow velocity increasing.
- The velocity of the liquid film increases with the air flow velocity increasing. The falling film flow velocity decreases along the circumferential direction in the middle plane, and increases in the right plane.

Acknowledgment

This work is supported by the National Natural Science Foundation of China (No. 51876026, No. 51776014). The authors would like to thank the anonymous reviewers for the helpful comments and suggestions related to this paper.

Symbols

A	—	Long semi-axis, mm
B	—	Short half-axis, mm
D	—	Tube diameter, mm
g	—	Gravitational acceleration, m/s^2
H	—	Tube spacing, mm
L	—	Distance from left liquid column, mm
L^*	—	Dimensionless distance
Re	—	Reynolds number
t	—	Time, s
V	—	Velocity, m/s
α	—	Volume fraction
λ	—	Whole length of the sheet mode, mm
ρ	—	Density, kg/m^3
σ	—	Surface tension, N/m
μ	—	Dynamic viscosity, kg/m s

Subscripts

g	—	Gas
l	—	Liquid

References

[1] X. Mu, S. Shen, Y. Yang, G. Liang, X. Chen, J. Zhang, Experimental study on overall heat transfer coefficient of seawater on three tube arrangements for horizontal-tube falling film evaporator, Desal. Wat. Treat., 57 (2016) 9993–10002.
[2] X. Mu, S. Shen, Y. Yang, X. Liu, Experimental study of falling film evaporation heat transfer coefficient on horizontal tube, Desal. Wat. Treat., 50 (2012) 310–316.
[3] S. Shen, G. Liang, Y. Guo, R. Liu, X. Mu, Heat transfer performance and bundle-depth effect in horizontal-tube falling film evaporators, Desal. Wat. Treat., 51 (2013) 830–836.
[4] S. Shen, H. Liu, L. Gong, Y. Yang, R. Liu, Thermal analysis of heat transfer performance in a horizontal tube bundle, Desal. Wat. Treat., 54 (2015) 1809–1818.
[5] H. Hou, Q. Bi, H. Ma, G. Wu, Distribution characteristics of falling film thickness around a horizontal tube, Desalination, 285 (2012) 393–398.
[6] Y. Han, N. Shikazono, Measurement of the liquid film thickness in micro tube slug flow, Int. J. Heat Fluid Flow, 30 (2009) 842–853.
[7] M. Fiorentino, G. Starace, Numerical investigations on two-phase flow modes in evaporative condensers, Appl. Therm. Eng., 94 (2016) 777–785.
[8] K.A. Jahangeer, A.A.O. Tay, M. Raisul Islam, Numerical investigation of transfer coefficients of an evaporatively-cooled condenser, Appl. Therm. Eng., 31 (2011) 1655–1663.
[9] L. Xu, S. Wang, Y. Wang, Y. Ling, Flowing state in liquid films over horizontal tubes, Desalination, 156 (2003) 101–107.
[10] K. Elshazly, M. Moawed, E. Ibrahim, M. Emara, Experimental investigation of natural convection inside horizontal elliptic tube with different angles of attack, Energy Convers. Manage., 47 (2006) 35–45.
[11] J.A. Esfahani, M. Modirkhazeni, Entropy generation of forced convection film condensation on a horizontal elliptical tube, C. R. Mec., 340 (2012) 543–551.
[12] C. Qi, H. Feng, H. Lv, C. Miao, Numerical and experimental research on the heat transfer of seawater desalination with liquid film outside elliptical tube, Int. J. Heat Mass Transfer, 93 (2016) 207–216.
[13] Q. Qiu, X. Zhang, X. Zhu, S. Quan, S. Shen, Influential analysis of geometrical parameters on falling-film thickness and distribution of sheet flow outside horizontal tube, Desal. Wat. Treat., 124 (2018) 98–105.
[14] Q. Tan, B. Jiang, Analysis of falling film flow and heat transfer characteristics outside the elliptical horizontal tube, J. Eng. Thermal Energy Power, 32 (2017) 20–25, 114.
[15] T. Peng, Y. Zhou, H. Hu, Z. Yan, Research on the thickness of falling liquid film outside horizontal semi-elliptical tubes with digital image processing, J. Eng. Thermophys., 39 (2018) 2040–2047.
[16] M. Asbik, O. Ansari, B. Zeghmati, Numerical study of boundary-layer transition in flowing film evaporation on horizontal elliptical cylinder, Numer. Heat Transfer, Part A: Applications, 48 (2005) 645–669.
[17] Y.T. Lee, S. Hong, C. Dang, L.H. Chien, L.W. Chang, A.S. Yang, Heat transfer characteristics of obliquely dispensed evaporating falling films on an elliptic tube, Int. J. Heat Mass Transfer, 132 (2019) 238–248.